Contrib Mineral Petrol (2016) 171:44
DOI 10.1007/s00410-016-1254-8

ORIGINAL PAPER

A systematic evaluation of the Zr-in-rutile thermometer in ultra-high temperature (UHT) rocks

Jonas Pape[1] · Klaus Mezger[1] · Martin Robyr[2]

Received: 24 November 2015 / Accepted: 25 March 2016

Abstract The Zr-in-rutile geothermometer is potentially a widely applicable tool to estimate peak metamorphic temperatures in rocks from diverse geological settings. In order to evaluate its usefulness and reliability to record and preserve high temperatures in granulite facies rocks, rutile from UHT rocks was investigated to assess different mechanisms of Zr (re-)distribution following cooling from high temperature. Granulite facies paragneisses from the lowermost part of the Ivrea Zone, Italy, incorporated as thin sheets into the extensive basaltic body of the Mafic Complex were selected for this study. The results show that Zr-in-rutile thermometry, if properly applied, is well suited to identify and study UHT terranes as it preserves a record of temperatures up to 1190 °C, although the thermometer is susceptible to partial post-peak metamorphic resetting by Zr diffusion. Texturally homogeneous rutile grains preserve Zr concentrations corresponding to temperatures of prograde rutile growth. Diverse rutile textures and relationships between some rutile host grains and included or adjacent Zr-bearing phases bear testimony to varying mechanisms of partial redistribution and resetting of Zr in rutile during cooling and link Zr-in-rutile temperatures to different steps of the metamorphic evolution. Rutile grains that equilibrated their Zr concentrations at temperatures above 1070 °C (i.e. 1.1 wt% Zr) could not retain all Zr in the rutile structure during cooling and exsolved baddeleyite (ZrO_2). By subsequent reaction of baddeleyite exsolution lamellae with SiO_2, zircon needles formed before the system finally closed at 650–700 °C without significant net loss of Zr from the whole host rutile grain. By reintegration of zircon exsolution needles, peak metamorphic temperatures of up to 1190 °C are derived for the studied rocks, which demonstrates the suitability of this solution thermometer to record UHT conditions and also confirms the extraordinary geological setting of the lowermost part of the Ivrea Zone.

Keywords Zr-in-rutile thermometer · Ultra-high temperature metamorphism · Ivrea Zone · Zircon/baddeleyite exsolution · Diffusion · Granulite facies

Introduction

The empirically and experimentally calibrated Zr-in-rutile geothermometer (Zack et al. 2004a; Watson et al. 2006; Tomkins et al. 2007) holds great potential to identify and investigate ultra-high temperature (UHT) metamorphic terranes (e.g. Luvizotto and Zack 2009; Meyer et al. 2011; Kooijman et al. 2012; Ewing et al. 2013, Korhonen et al. 2014). Conventional geothermometry based on element exchange reactions between two phases is very susceptible to post-peak diffusional resetting and thus might underestimate peak temperatures, especially for UHT conditions. Furthermore, for exchange thermometry, both phases involved in the reaction need to be stable at UHT conditions, which for many mineral pairs is often not the case.

Communicated by Jochen Hoefs.

Electronic supplementary material The online version of this article (doi:10.1007/s00410-016-1254-8) contains supplementary material, which is available to authorized users.

✉ Jonas Pape
jonas.pape@geo.unibe.ch

[1] Institute of Geological Sciences, University of Bern, Baltzerstrasse 1+3, 3012 Bern, Switzerland

[2] Institute of Earth Sciences, University of Lausanne, UNIL-Mouline, 1015 Lausanne, Switzerland

Published online: 19 April 2016

For these reasons, the identification of UHT terranes and of the peak temperatures they may have attained are commonly based on P–T pseudosection calculations and on the appearance or the absence of critical mineral parageneses.

The Zr-in-rutile thermometer is an excellent alternative when searching for ancient UHT terranes and investigating their equilibration temperatures. However, it can only be a powerful tool, if its behaviour at UHT conditions is known. The application of the Zr-in-rutile geothermometer is straightforward as it is mainly based on the temperature-dependent incorporation of Zr as a trace element into rutile in the presence of quartz and zircon. Rutile is a common accessory mineral in a wide variety of high-grade metamorphic rocks including those from UHT environments. The thermodynamic basis of the temperature-dependent incorporation of Zr into the rutile structure is quite simple (e.g. Watson et al. 2006; Ferry and Watson 2007). Nevertheless, over the last decade, numerous studies have shown that the incorporation of Zr into rutile and its resetting under geological conditions is a more complex process than originally thought when considering the thermodynamic parameters exclusively. Temperature data from the Zr-in-rutile thermometer can thus be challenging to interpret correctly in a geological context, especially for HT and UHT samples (e.g. Zack et al. 2004a; Luvizotto and Zack 2009; Kooijman et al. 2012; Ewing et al. 2013; Smye and Stockli 2014). Commonly, Zr is homogenously distributed in rutile crystals, but its concentration can range from a few hundred to several thousand μg/g between different rutile grains within the same thin section, resulting in a spread of several 100 °C in the estimated Zr-in-rutile temperatures for the same rock sample. Explanations for this intergranular variations of Zr contents include: (1) the preservation of primary Zr concentrations from rutile growth at different temperatures during the prograde metamorphic evolution; (2) rutile recrystallization or resetting by diffusion and re-equilibration of Zr concentrations during subsequent retrograde metamorphic stages (e.g. Luvizotto and Zack 2009); and (3) a combination of both mechanisms. For a robust interpretation of Zr-in-rutile temperatures, it is consequently essential to establish which of these mechanisms controls the behaviour of Zr in rutile. Since large intergranular spreads of Zr concentrations in rutile are particularly well documented in UHT rocks, this study focuses on the understanding of the behaviour of Zr in rutile from granulite facies rocks for which the peak metamorphic temperature can be estimated independently. For this purpose, the Ivrea Zone in north-west Italy provides excellent rutile-bearing high and ultra-high temperature rocks from the lower continental crust. Metapelitic xenoliths metamorphosed by the surrounding gabbroic melt of the Mafic Complex in the Ivrea Zone were selected for a detailed study to constrain the behaviour of Zr in rutile under extreme temperature conditions. It can be shown that the Zr-in-rutile thermometer, if applied to UHT rocks, is susceptible to post-peak metamorphic redistribution and resetting of Zr by different processes such as exsolution and diffusion. However, if applied properly, it indeed records prograde metamorphism and UHT conditions, and by reintegration of zircon exsolutions, it recovers exceptionally high temperatures reflecting the extraordinary geological setting of the lower part of the Ivrea Zone.

Geological setting

The Ivrea Zone exposed in north-west Italy corresponds to a cross section through the Adriatic lower continental crust that was subsequently uplifted and tilted during the Alpine orogeny (Barboza et al. 1999; Quick et al. 1995; Sinigoi et al. 1995; Zingg 1980). The Ivrea Zone can be subdivided into two major units—the Kinzigite Formation and the Mafic Complex (Quick et al. 2003; Fig. 1). Zingg (1980) was one of the first who clearly identified critical mineral reactions and mineral isograds providing first evidence for granulite facies metamorphism in the lower parts of the Ivrea Zone.

The Kinzigite Formation consists mainly of amphibolite to granulite facies paragneisses, which include dominantly metamorphosed wackes, metapelites, marbles and mafic rocks (Quick et al. 1995). An important mineral reaction within the amphibolite to granulite facies metapelitic rocks of the Kinzigite Formation is the breakdown of biotite and the formation of garnet and K-feldspar by the reaction Bt + Sil + Qtz = Grt + Kfs + H_2O, which led to an increasing amount of garnet over biotite in the granulite facies metapelites of the Ivrea Zone. Additionally, the breakdown of high-Ti biotite released Ti, which enabled the formation of rutile (Luvizotto and Zack 2009; Schnetger 1994; Zingg 1980). For this reason, rutile-bearing metapelites are mainly found in K-feldspar + garnet-bearing gneisses of the Ivrea Zone. The dehydration reaction liberates H_2O and thereby decreases the melting temperature of crustal rocks. Widespread anatexis in the lower part of the Ivrea Zone consequently resulted in strongly restitic metapelites depleted in trace elements (Schnetger 1994) and enriched in garnet and up to one mm large rutile crystals.

The Mafic Complex consists of an extensive body of mafic rocks, which underlies the Kinzigite Formation. Its evolution is interpreted as resulting from a thermal event related to widespread lithospheric thinning during Permo-Carboniferous time (Barboza and Bergantz 2000; Schuster and Stüwe 2008). The main magmatic event and the emplacement of the major part of the Mafic Complex have been dated with U–Pb in zircon at 288 ± 4 Ma (Peressini et al. 2007). The occurrence of small slices of the Mafic

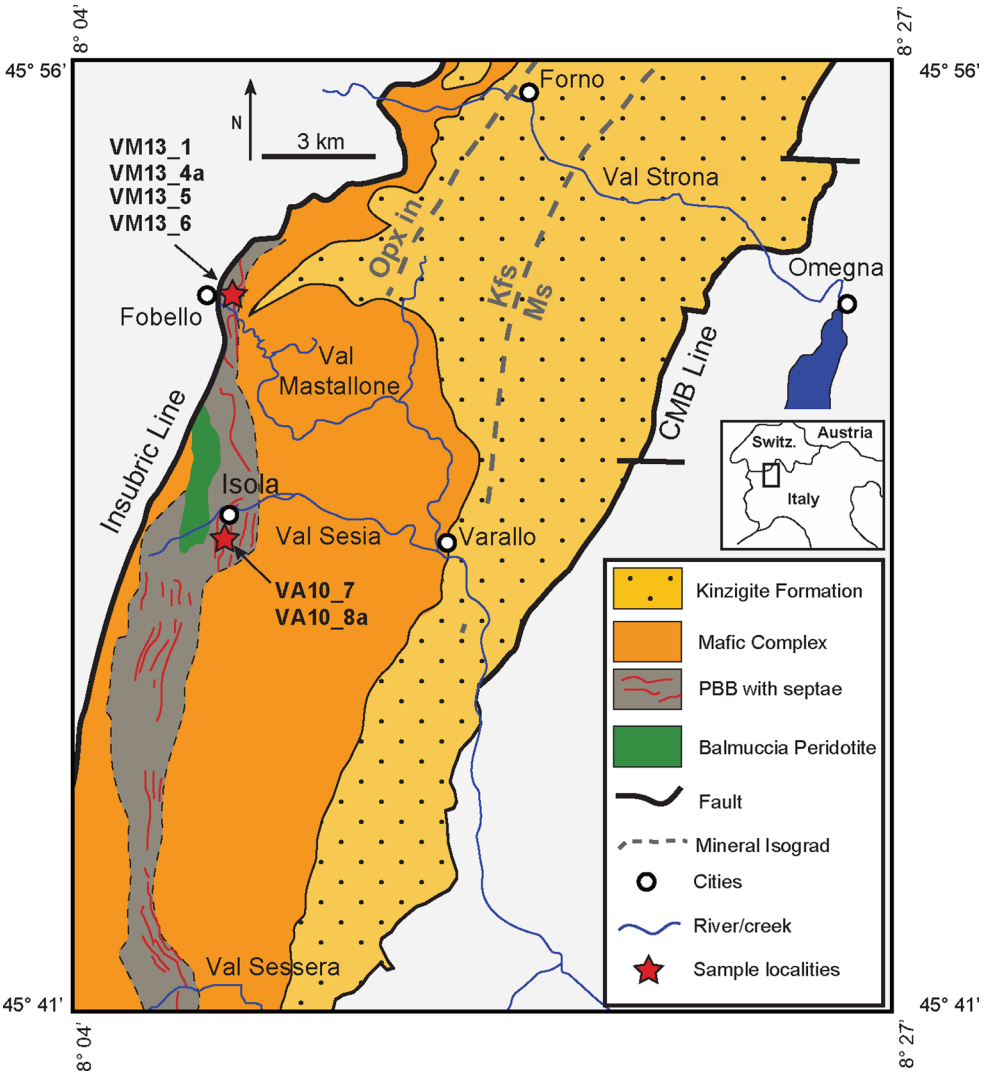

Fig. 1 Geological map of the Ivrea Zone, NW Italy, showing the two main units of the IZ. The *red stars* mark the sample localities near Isola (Val Sesia) and Fobello (Val Mastallone) within the paragneiss-bearing belt (PBB) in the Mafic Complex. Modified after Barboza and Bergantz (2000), Meyer et al. (2011) and Ewing et al. (2013)

Complex along the Insubric Line, which separates the Ivrea Zone from the Central Alps (Fig. 1), with distinct texture and composition suggests that the Mafic Complex did not intrude within or underplated the lower continental crust in a short-term single-step event, but rather resulted from several successive intrusions (Barboza and Bergantz 2000). The Mafic Complex includes gabbros and norites and few small lenses of mantle peridotite. Additionally, it contains thin elongated sheet-like lenses of metapelitic rocks, so-called paragneiss septae (Sinigoi et al. 1996), which are clustered within the 'paragneiss-bearing belt' (PBB) (Sinigoi et al. 1995; Fig. 1). They range in thickness from a few dm to 100 m and are interpreted as slices of the lowermost crustal rocks of the Kinzigite Formation (Quick et al. 1995) that were incorporated into the Mafic Complex during its emplacement (Sinigoi et al. 1995). These highly restitic, metapelitic rocks have been consequently exposed to the melting temperature of basalt i.e. up to ca. 1200 °C and are particularly suitable to study the behaviour of the Zr-in-rutile thermometer at UHT conditions. The gneisses generally consist of quartz, feldspar, garnet, sillimanite, orthopyroxene ± rutile ± zircon ± biotite ± corundum ± graphite (Quick et al. 2003). In comparison with the granulite facies paragneisses of the Kinzigite Formation, they show a higher abundance of garnet and a lower abundance of biotite.

Thermal conditions for mineral equilibration in the metapelites of the Kinzigite Formation have been estimated by classical geothermometry using the Fe–Mg exchange between garnet and biotite (Henk et al. 1997). The resulting temperature estimates of ~600 to ~810 °C for rocks from Val Strona record the increasing metamorphic conditions in the Kinzigite Formation towards the Mafic Complex (Fig. 1). More recent Zr-in-rutile temperatures (Luvizotto and Zack 2009) and P–T estimates by pseudosection calculations (Redler et al. 2012) for similar transects give significantly higher peak temperatures of ca. 850–950 °C. These higher temperatures indicate the susceptibility of Fe–Mg

exchange thermometry to post-peak resetting by diffusion and thus potentially underestimates peak metamorphic conditions—at least for granulite facies rocks. Even higher temperatures are expected for the septae that were completely enclosed in the basaltic melts of the Mafic Complex. Zr-in-rutile temperatures of 1000–1020 °C are so far the only temperature estimates for the Val Mastallone septae (Ewing et al. 2013). For the Val Sesia septae, temperature estimates are presented in this study for the first time.

Methods

Imaging by scanning electron microscopy (SEM)

Backscatter electron (BSE) and secondary electron (SE) images were performed using a scanning electron microscope (SEM) ZEISS EVO50 instrument at the Institute of Geological Sciences, University of Bern. Acceleration voltage was set between 15 and 20 kV, and the beam current ranged from 500 pA to 2000 nA at high vacuum conditions. All thin sections were carbon-coated.

Electron microprobe analysis (EMPA) and Zr-in-rutile temperatures

To quantify the chemical composition of rutile, EMP analyses were carried out at the Institute of Geological Sciences, University of Bern, using a JEOL JXA-8200 Superprobe. Rutile grains were analysed in polished and carbon-coated thin sections (~30 µm). Acceleration voltage and beam current were set at 15 kV and 100 nA, respectively, for all measurements. A focused beam with a spot size of ~1 µm was used for spot analyses. For line analyses, the spot size was set at 5 µm during a first session and 1 µm for a second session.

Some rutile grains containing zircon exsolution needles were additionally analysed by EMP using a defocused 60 µm beam diameter. Depending on rutile grain size, up to 20 defocused spots were set on individual rutile grains in order to cover whole grains for analytical reintegration of zircon needles of Type-II rutile grains.

The concentrations of Si, Zr, Nb, Cr, Al, Ti, V and Fe were analysed using five wavelength-dispersive X-ray spectrometers (WDS). X-ray intensities were determined on Kα lines (Si, Cr, Al, Fe, Ti, V) and Lα lines (Nb, Zr) using the spectrometer crystals TAP (Si), PETH (Zr), LIF (Cr), PETL (Nb), TAPH (Al), PET (Ti, V) and LIFH (Fe). The X-ray peak and background intensities of Cr, Nb, Al, Fe and V were measured for 150 and 75 s, respectively, intensities of Si for 30 and 15 s, of Ti for 20 and 10 s and of Zr for 300 and 150 s. The detection limit for Zr was about 40 µg/g. For all the other elements, the detection limit was between 40 and 100 µg/g. Automated matrix correction was done according to the CITZAF package (Armstrong 1995). Interference of Ti Kβ X-rays on the V Kα line was corrected offline using a previously determined correction factor. Because this correction provokes a higher uncertainty on the resulting concentrations of V, the absolute V concentrations were not further evaluated. Vanadium concentration profiles are still useful, since evaluation of potential concentration gradients (e.g. due to diffusion) is not affected by the high systematic uncertainty introduced by the interference correction.

To identify analyses of micro-inclusions such as zircon exsolution needles, Si was used as a monitoring element for all analyses. Measurements with Si > 300 µg/g and anomalously high Zr contents were discarded. Obviously, this method is suitable for zircon inclusions but is not appropriate for baddeleyite exsolutions. In order to minimize this issue, all rutile grains were carefully studied by SEM and Raman spectroscopy prior to the EMP analyses.

EMP line profiles were measured in two different analytical sessions. In order to obtain a good spatial resolution along the quantitative profiles towards rutile grain boundaries, the measurements of the first session were performed as overlapping point measurements with a defocused beam of 5 µm and a step size of 2.5 µm. In a second session, line profiles were measured with a focused beam of 1 µm and a step size of 3 µm.

Altogether, more than 550 individual points on ~150 rutile grains from six hand specimens were analysed by EMP. The chemical composition of rutile grains was determined on the basis of two to four point measurements on each grain. The results were then carefully checked for homogeneity and precision of the concentrations of measured trace elements. In case of homogeneous and consistent data on single grains, the point measurements were averaged to calculate mean values for all elements. These weighted mean results were subsequently used for temperature calculations. Pressures of 8–10 kbar are assumed for the samples collected from both the Val Sesia and the Val Mastallone septae and are similar to previously published pressure estimates for Val Mastallone (Ewing et al. 2013). Zr-in-rutile temperatures that are calculated for these estimated pressures generally do not differ significantly for the two different calibrations of Watson et al. (2006) and Tomkins et al. (2007). All Zr-in-rutile temperatures presented in this study are calculated using the calibration of Watson et al. (2006).

Error estimation for Zr measurements and Zr-in-rutile temperatures

The successful calibration of Zr measurements using EMP was confirmed by additional analyses performed on the secondary natural rutile standard R10b (see Supplementary). Based on the results of repeated measurements on R10b, an

analytical uncertainty of ±10 % for low Zr concentrations (i.e. <1000 µg/g) is assigned to the microprobe measurements. For the sake of simplicity, this analytical uncertainty was also assigned to high Zr concentrations, even though the true uncertainties for high Zr rutiles (i.e. >1000 µg/g) are significantly smaller. The uncertainties of the final Zr-in-rutile temperatures were calculated based on Gaussian error propagation considering the analytical uncertainty and the uncertainties inherent in the equation of Watson et al. (2006), and result in ±5.0–5.3 % error on the calculated Zr-in-rutile temperatures over the temperature range of interest (i.e. 600–1100 °C).

Mathematical reintegration of zircon exsolutions

Zirconium contents of zircon needles, which are interpreted as exsolutions, were reintegrated to obtain Zr contents of the rutile host grains prior to exsolution. First, rutile grains were analysed by EMP-focused beam measurements for the Zr contents of the grain matrix. Subsequently, BSE/SE-microphotographs were used to quantify the volume percent of exsolved phases based on their 2-dimensional distribution for each grain. This was done by pixel counting using an image editing software. Care was taken to only include rutile grains with absolutely regular and evenly distributed zircon exsolution needles. For the following calculations, the exsolved zircon needles were assumed to be stoichiometric with 67.2 wt% ZrO_2 or 49.75 wt% Zr. Densities used for the calculations were 4.25 and 4.60 g/cm^3 for rutile and zircon, respectively. The calculations are based on the following equation

$$Zr_{int} = \frac{[(Vol\%_{Rt\text{-}h} * \rho_{Rt} * Zr_{Rt\text{-}h}) + (Vol\%_{Zrn\text{-}x} * \rho_{Zrn} * Zr_{Zrn})]}{[(Vol\%_{Rt\text{-}h} * \rho_{Rt}) + (Vol\%_{Zrn\text{-}x} * \rho_{Zrn})]}$$

where $Vol\%_{Rt\text{-}h}$ is the percent by volume of the rutile host grain, ρ_{Rt} is the density of rutile in g/cm^3, $Zr_{Rt\text{-}h}$ is the Zr content of the matrix of the rutile host grain in µg/g, $Vol\%_{Zrn\text{-}x}$ is the percent by volume of the exsolved phase, ρ_{Zrn} is the density of zircon in g/cm^3 and Zr_{Zrn} is the Zr content of stoichiometric zircon in µg/g.

Samples

The set of samples comprises six hand specimens of metapelitic rocks from two different paragneiss septae from the Val Sesia and the Val Mastallone (Fig. 1). The samples VA10_7 and VA10_8a were taken from a few metre wide paragneiss septae along a feeder creek of the Val Sesia River south of the village of Isola (Fig. 1, Table S2). The samples VM13_1 to VM13_6 were collected from a paragneiss septae outcropping in the Val Mastallone along the Mastallone creek and along the Strada Provinciale 9, about 1 km south-east of the village of Fobello (Fig. 1, Table S2).

All samples show a similar mineral assemblage with garnet as main mineral phase associated with rutile + zircon + quartz, which is the critical paragenesis for temperature estimates using the Zr-in-rutile thermometer. Orthopyroxene, sillimanite and quartz are present in samples from Val Sesia suggesting UHT metamorphism (e.g. Harley 1989), although not displaying a paragenetic relationship in thin section. In addition, low Zn hercynitic spinel + quartz and the occurrence of perthitic feldspar in some of the samples indicate UHT conditions. Sillimanite is present in all but two samples indicating HT. All samples are only weakly altered and commonly contain abundant and large rutile, mostly consisting of 20–900 µm subhedral to euhedral crystals. Some gneiss samples show a layered structure with restitic, garnet-rich layers and leucocratic layers. Rutile grains can be found in both, the matrix assemblage and as inclusions within garnet, pyroxene or quartz.

The investigated rutile grains show a large range in sizes, shapes and also in their textures. In thin sections, some grains are featureless in transmitted and reflected light, showing no alteration, no degradation and no reactions with other phases. In contrast, some other grains enclose or are intergrown with ilmenite crystals, or show partial pseudomorphic replacement of rutile by ilmenite.

Rutile types and Zr-bearing phases within or adjacent to rutile

Many rutile grains occur intimately associated with Zr-bearing phases (Figs. 2, 3). These phases were identified by Raman spectroscopy (Fig. 4) and EMP elemental mapping to be commonly zircon, although baddeleyite may be present in rare cases (Fig. 2f). Due to the small size of the exsolutions, Raman analyses never resulted in distinct spectra for host and inclusion but always revealed mixed spectra with the rutile host dominating (Fig. 4).

Zr-bearing phases closely associated with rutile occur (1) commonly as very tiny lamellae or needle-like exsolutions of baddeleyite or zircon in rutile (Figs. 2f, 3), which are only known from high-temperature (HT) and ultra-high temperature (UHT) samples (e.g. Harley and Motoyoshi 2000; Ewing et al. 2013) and provide strong evidence for redistribution of Zr in rutile; (2) as small rounded inclusions within rutile (Fig. 2b) or (3) as small and thin crystals adjacent to and rimming the rutile grains (Fig. 2b–e).

The differences in texture between rutile grains suggest multiple mechanisms for the redistribution of Zr in rutile, and play an important role, when discussing and interpreting the spread in Zr contents of rutile grains from single thin sections. Therefore, rutile grains are subdivided into three different groups depending on the type and textural relation with zircon or baddeleyite. It should be stressed that Zr-bearing phases within or adjacent to rutile can

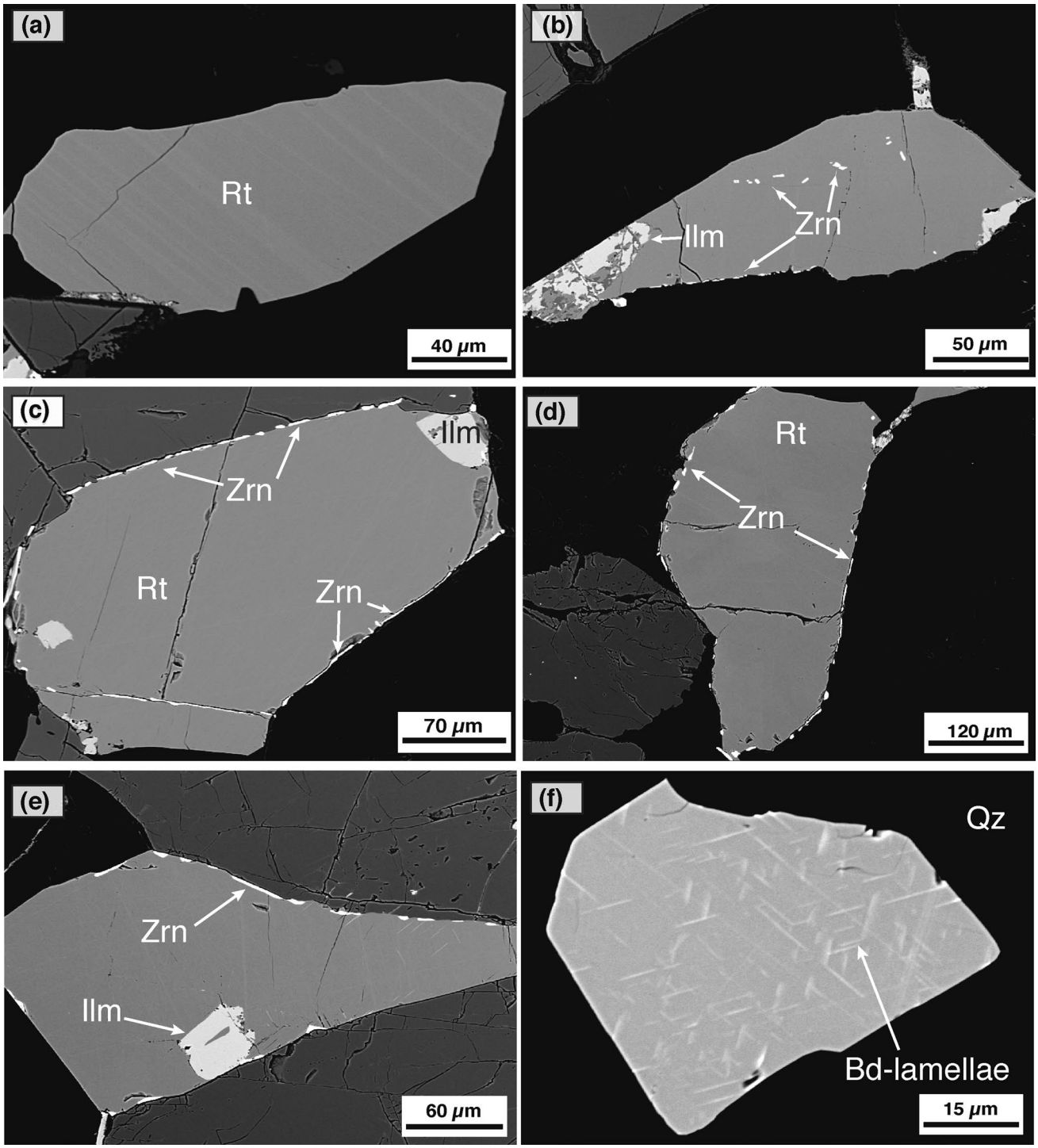

Fig. 2 Backscattered electron (BSE) images of rutile grains performed on a scanning electron microscope (SEM) showing **a** homogeneous (Type-I) rutile grain with minor replacement by ilmenite, **b** homogeneous unzoned rutile grain partially replaced by ilmenite, with some small zircon crystals at the lower grain edge and within the grain, **c**–**e** rutile grains (Type-III) with different amounts of small zircon crystals at the grain edges but a very homogeneous matrix, **f** Type-II rutile grain with regular exsolution lamellae of baddeleyite

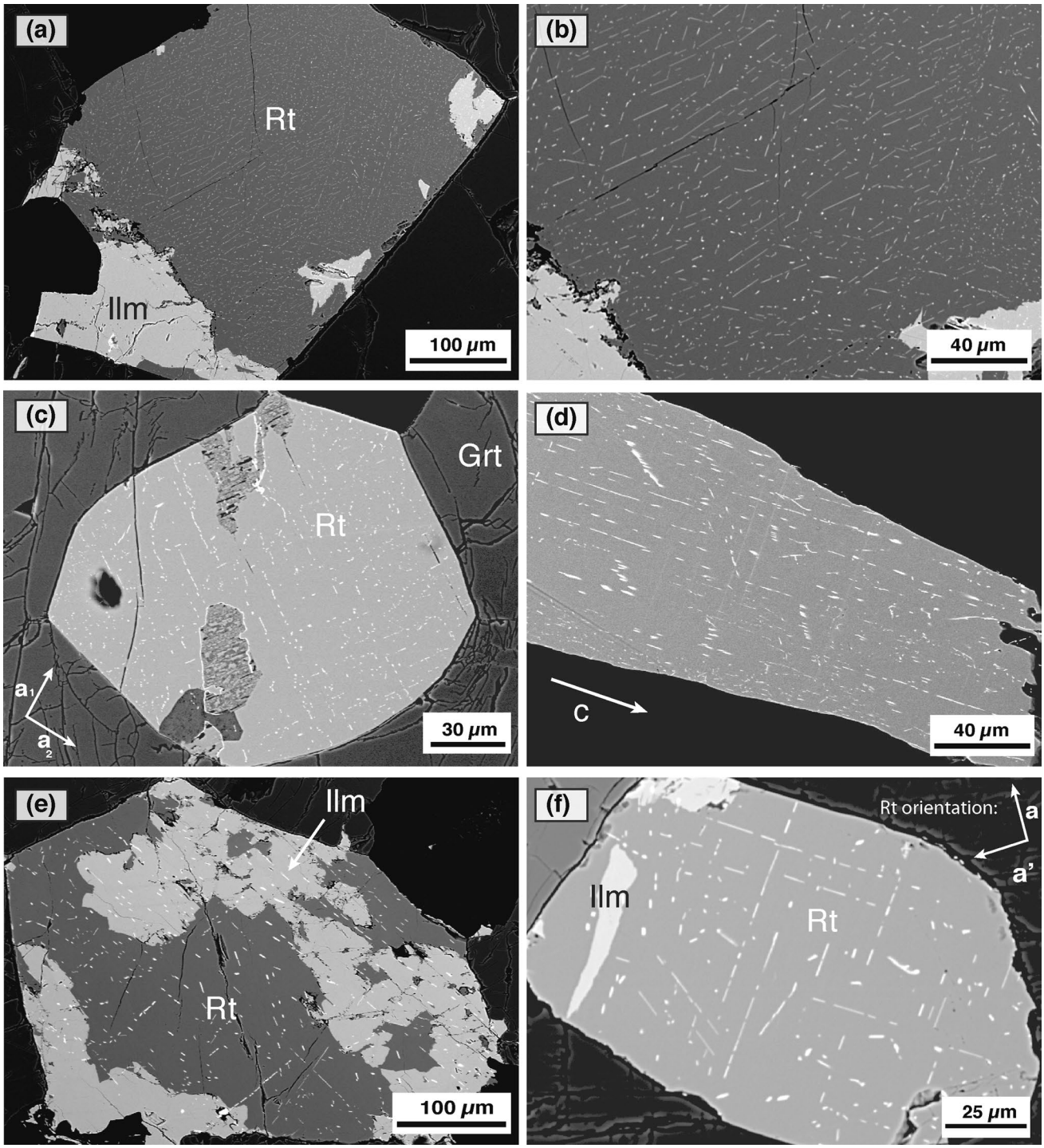

Fig. 3 Backscattered electron (BSE) images of rutile grains performed on a scanning electron microscope (SEM) showing **a** rutile grain partially replaced by ilmenite with regular, needle-like exsolution of zircon (Type-II rutile), **b** detail of the same rutile grain as **a** with preferred orientations of zircon exsolution needles in 2–3 directions, **c** rutile grain included within garnet, cut parallel to a_1 and a_2 axes, showing regular zircon exsolution needles in two preferred orientations, **d** rutile grain cut parallel c showing regular zircon exsolution needles in the direction of the *c*-axis, **e** rutile grain partially replaced by ilmenite with zircon exsolution needles stretching across the rutile–ilmenite grain boundary, **f** rutile grain with regular zircon exsolution needles showing three preferred orientations and granular zircon within the matrix

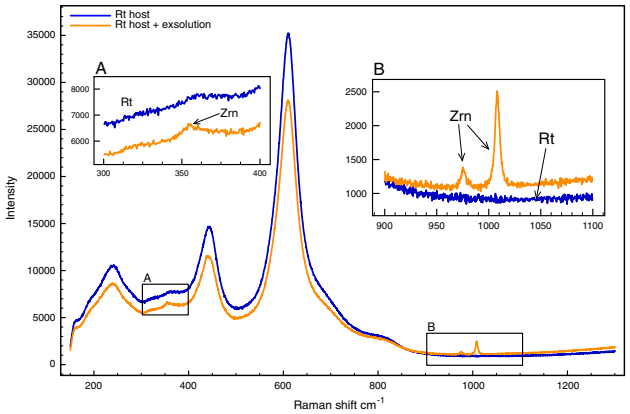

Fig. 4 Raman spectra of Rt host (*blue*) and Rt host + Zrn inclusion (*orange*). Although the strong Rt signal predominates the spectra, two characteristic Zrn peaks at 975 and 1007 cm^{-1} (subwindow *B*) and a weaker Zrn peak at 355 cm^{-1} (subwindow *A*) are clearly visible

hardly be observed by optical microscopy, requiring detailed and careful scanning electron microscopy (SEM) investigations.

Type-I rutile, without textural relation with zircon or baddeleyite

About the half of the analysed rutile grains show no textural relation with zircon or baddeleyite. Neither do these rutile crystals contain zircon exsolutions or baddeleyite lamellae nor are they rimmed by zircon (e.g. Fig. 2a).

Type-II rutile, containing zircon exsolution needles or baddeleyite lamellae

About 10 % of all analysed rutile grains contain small zircon crystals that form elongated needle-like exsolutions (Fig. 3). The size of the zircon needles ranges from less than a µm in diameter to a few µm in length. In some cases, where rutile has been partly replaced by ilmenite, zircon exsolution needles cross the rutile–ilmenite grain boundary without any change in crystal size, shape or orientation (Fig. 3e). This indicates that ilmenite not only served as a source of TiO_2 to form rutile during prograde metamorphism (besides biotite), but rutile itself became replaced by ilmenite on the retrograde path after formation of zircon needles. The two major reactions responsible for the retrograde formation of ilmenite may be the GRIPS and GRAIL reactions Grs + 2Alm + 6Rt = 6Ilm + 3An + 3Qtz and Alm + Rt = Ilm + Sil/And + Qtz which are predominantly pressure sensitive, with the formation of ilmenite on the low-pressure side (Bohlen and Liotta 1986; Bohlen et al. 1983a). According to these two reactions, the breakdown of garnet and rutile leads to the formation of ilmenite during decompression. However, reaction textures directly pertaining to the two reactions were not identified in the thin sections.

Zircon needles in rutile commonly show shape-preferred orientations (SPO) in four directions controlled by the lattice of the host rutile, with two SPO orthogonal to each other parallel to {110} of the rutile host (Fig. 3c) and one SPO in the direction of the c-axis of the rutile host (Fig. 3j). One additional SPO of zircon needles is less abundant, but its crystallographic orientation could not be determined. The extinction behaviour in polarized light, which could give hints about the crystallographic orientations of the zircon needles, could not be examined by optical microscopy, because the crystals are too small.

One rutile grain was found to preserve baddeleyite exsolution lamellae (Fig. 2f). In contrast to the needle-like zircon exsolutions, baddeleyite lamellae occur as more continuous sheet-like structures displaying rather faint boundaries with the rutile host. Baddeleyite lamellae show shape-preferred orientations in three directions. As for the zircon exsolution needles, extinction behaviour of baddeleyite lamellae could not be examined by optical microscopy due to the small size of the crystals.

Type-III rutile, containing granular zircon inclusions or with granular zircon along grain margins

Numerous rutile grains contain small rounded, drop-like µm-sized zircon crystals that show no evidence for SPO. Clusters of several of these zircon grains can be observed locally in the rutile host, whereas other zircon grains are randomly distributed in the host grain (Figs. 2b, 3f). The extinction behaviour of granular zircon within rutile could not be examined by optical microscopy. Thus, evidence of crystallographic preferred orientation (CPO) is not given.

A more common feature of many rutile grains is the occurrence of numerous and thin zircon crystals along the grain edges. Some of these small, typically 2–4 µm thick, zircon crystals are elongated, rimming almost the whole rutile grain (Fig. 2c, d). In some cases, the zircon crystals rim the rutile crystals only locally (Fig. 2b, e). A systematic correlation between the textural arrangement of the zircon rimming rutile and the adjacent major mineral phases in the matrix is not obvious.

Results

Trace elements in rutile

Within single samples, Zr concentrations range from 271 to 7650 µg/g (VA10_7), 266–6274 µg/g (VA10_8a), 317–11228 µg/g (VM13_1), 308–8735 µg/g (VM13_4a),

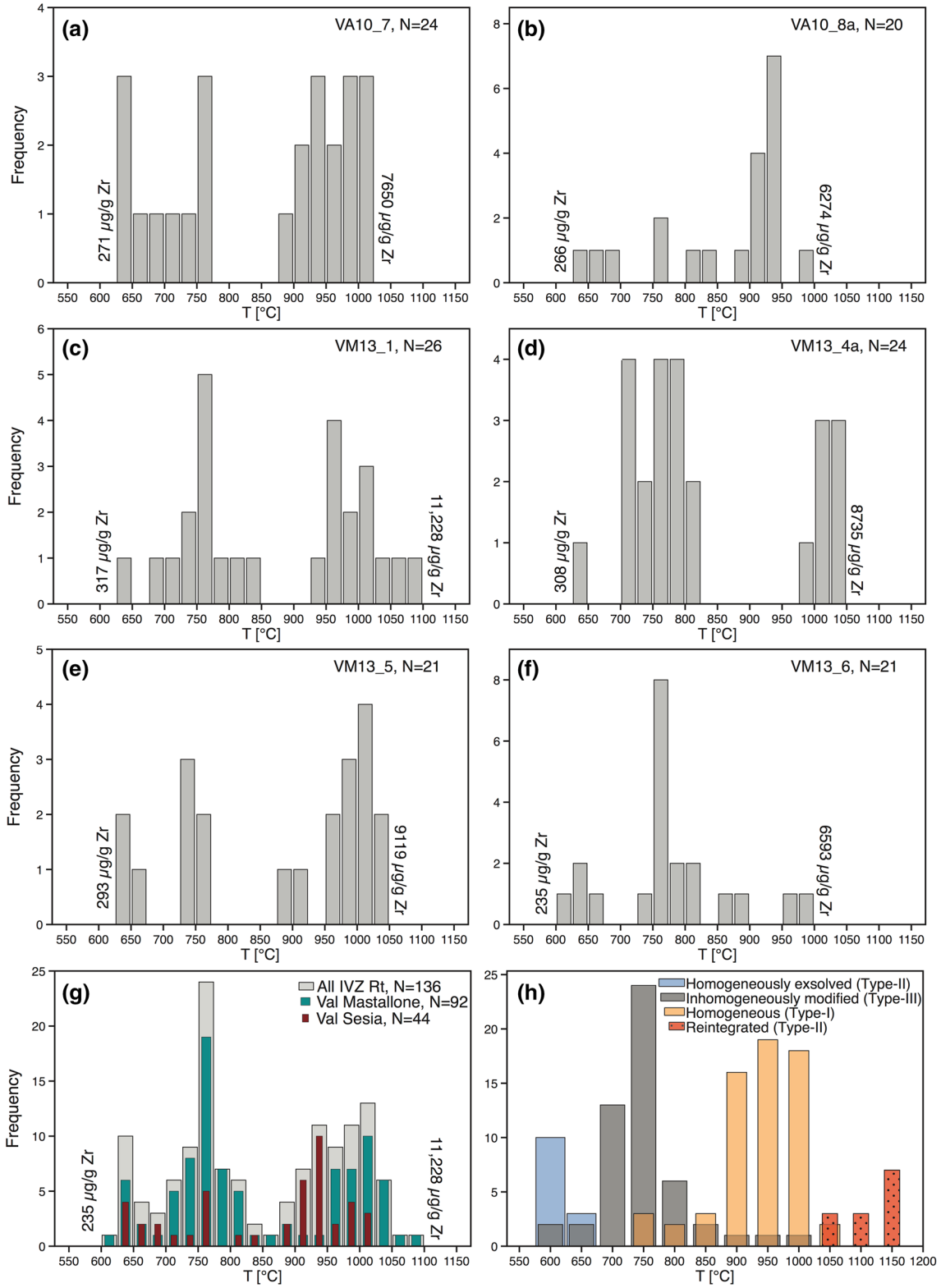

Fig. 5 Temperature frequency histograms of samples **a** VA10_7 and **b** VA10_8a from Val Sesia and samples **c** VM13_1, **d** VM13_4a, **e** VM13_5, and **f** VM13_6 from Val Mastallone. Some samples (VA10_7, VM13_1, VM13_4a and VM13_5) show distinct bimodal temperature distributions. The histogram (**g**) pools the results based on sample locality; in figure **h** samples are grouped based on textural differences (see text for details)

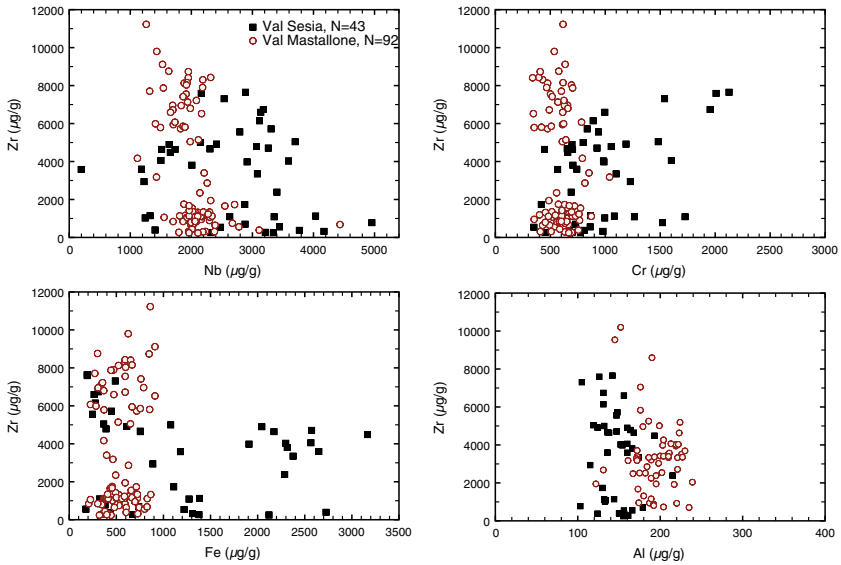

Fig. 6 Zr versus Nb, Cr, Fe and Al. Data are distinguished by their locality

Table 1 Data used for and results of mathematical reintegration of Zr contents of zircon exsolution needles

Sample	$Vol\%_{Rt\text{-}h}$	$Vol\%_{Zrn\text{-}x}$	$Zr_{Rt\text{-}h}$ (μg/g)	Zr_{int} (wt%)	$T_{Rt\text{-}h}$ (°C)	$T_{integrated}$ (°C)
VA10_7_gRt8	96.9	3.1	321	1.68	648	1153
VA10_7_gRt9	97.5	2.5	375	1.35	661	1112
VA10_7_gRt11	96.6	3.4	250	1.85	628	1172
VA10_7_gRt12	97.9	2.1	271	1.17	634	1085
VA10_7_Rt1	96.3	3.7	558	2.06	696	1194
VA10_8a_Rt5	97.5	2.5	266	1.36	633	1113
VM13_4a_Rt19	97.7	2.3	308	1.25	645	1096
VM13_5_Rt3	97.8	2.2	313	1.24	646	1095
VM13_5_Rt7	96.8	3.2	293	1.75	641	1161
VM13_5_Rt16	96.3	3.7	438	2.04	674	1192
VM13_6_Rt4	96.8	3.2	235	1.76	623	1162
VM13_6_Rt13/1	96.4	3.6	269	1.97	634	1186
VM13_6_Rt15	97.0	3.0	244	1.63	626	1147

293–9119 μg/g (VM13_5) and 235–6593 μg/g (VM13_6) (Fig. 5a–f). The Zr concentration of all analysed rutile grains ranges from 235 to 11,228 μg/g (Fig. 5g). Niobium concentration of all analysed grains ranges from 200 to 5000 μg/g and Cr concentration from 340 to 2100 μg/g (Fig. 6). The Fe content of the Val Mastallone samples ranges from 200 to 1000 μg/g, whereas the Fe content of the Val Sesia samples ranges from 200 to 3500 μg/g (Fig. 6). The rutile grains included in garnet typically contain more than 1000 μg/g Fe. With Al concentrations from ~100 to 200 μg/g, the rutiles from Val Sesia show concentrations very similar to Val Mastallone samples which contain between ~120 and 250 μg/g of Al (Fig. 6). The samples from the Val Sesia display generally a larger spread in Nb, Cr and Fe compared to those from the Val Mastallone (Fig. 6). Aluminium, Fe, Nb and Cr do not correlate systematically with Zr (Fig. 6).

Zr-in-rutile temperatures

The calculated Zr-in-rutile temperatures for the focused beam EMP analyses are plotted in temperature histograms using a bin size of 25 °C which also corresponds to the estimated absolute error on low Zr-in-rutile temperatures. Four out of six samples show a bimodal distribution of Zr, and consequently two groups of temperatures can be derived with the Zr-in-rutile thermometer (Fig. 5). The first group provides temperatures from ~650 to 750 °C (VA10_7) (Fig. 5a), 750 to 800 °C (VM13_1, VM13_4a) (Fig. 5c, d) and ~700 to 750 °C (VM13_5) (Fig. 5e), whereas the other

group records temperatures from ~900 to 1000 °C for the Val Sesia samples and 950 to 1050 °C for the samples from the Val Mastallone (Fig. 5g). A general trend shows that the samples from the Val Sesia display a well-defined high temperature cluster around 900–1000 °C and a more poorly defined cluster around 750–800 °C (Fig. 5g). The Val Mastallone samples record both, a distinct high temperature cluster around 950–1050 °C and a pronounced low temperature cluster around 700–800 °C (Fig. 5g). Combining all Zr-in-rutile temperatures of all analysed Ivrea Zone rutile, the resulting frequency histogram shows three distinct temperature clusters at ~640, 760 and 1000 °C (Fig. 5g).

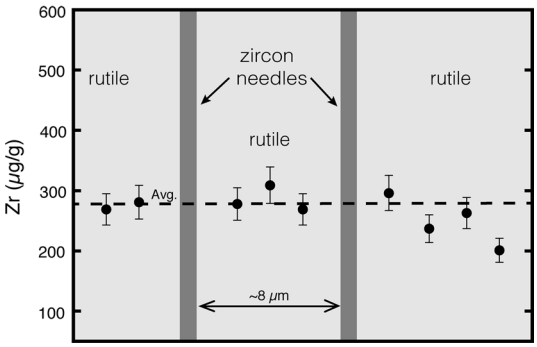

Fig. 7 Zirconium concentration profile within rutile grain gRt9 between and adjacent to zircon needles showing no decrease or systematic variations in Zr concentrations towards the zircon needles. Within uncertainty, Zr concentrations are identical. See text for further explanations

Mathematical and analytical reintegration of zircon exsolution needles

The zircon exsolution needles of 13 Type-III rutile grains were mathematically reintegrated to obtain the initial Zr content of the rutile host grains prior to the exsolution (Table 1). All rutile grains have low matrix Zr concentrations of ~250–550 µg/g resulting in Zr-in-rutile temperatures of 600–700 °C. EMP concentration profiles between these exsolutions reveal that between zircon exsolution needles, the Zr concentration is homogenous (Fig. 7). The volume of exsolved zircon is always between 2 and 4 %, so that reintegration of the Zr content of zircon exsolution needles shifts the Zr concentration for the rutile host grains to ~1.2–2 wt% and thus Zr-in-rutile temperatures to 1080–1200 °C (Table 1). The analytical reintegration by defocused beam measurements on the same rutile grains as used for mathematical reintegration results in systematically

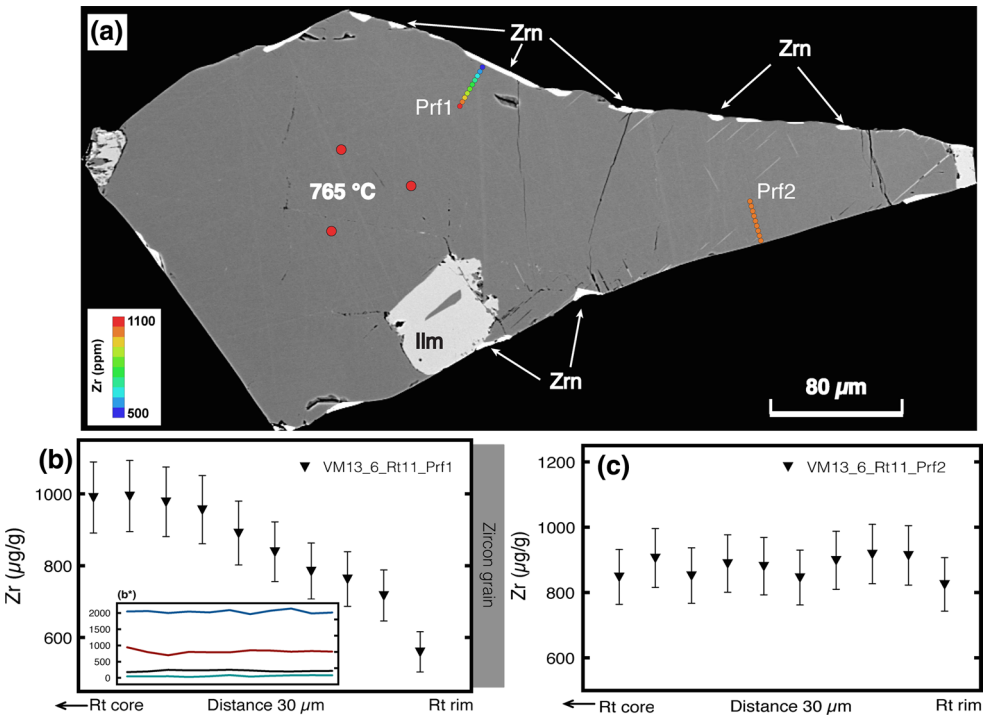

Fig. 8 **a** Backscattered electron image of rutile grain Rt11 of sample VM13_6. The EMP concentration profiles VM13_6_Rt11_Prf1 and VM13_6_Rt11_Prf2 are drawn in and show the systematic decrease of Zr in rutile towards adjacent zircon and the flat Zr profile towards the rutile grain edge without zircon. **b** Concentration profile VM13_6_Rt11_Prf1 towards adjacent zircon showing the systematic decrease of Zr towards the zircon grain. Subwindow *b** shows the constant concentration profiles of Si (teal), Al (black), Cr (*red*) and Nb (*blue*) over the same distance as for Zr. **c** The profile VM13_6 Rt11_Prf2 was set within the same grain but towards rutile grain boundaries without adjacent zircon and shows constant Zr concentrations

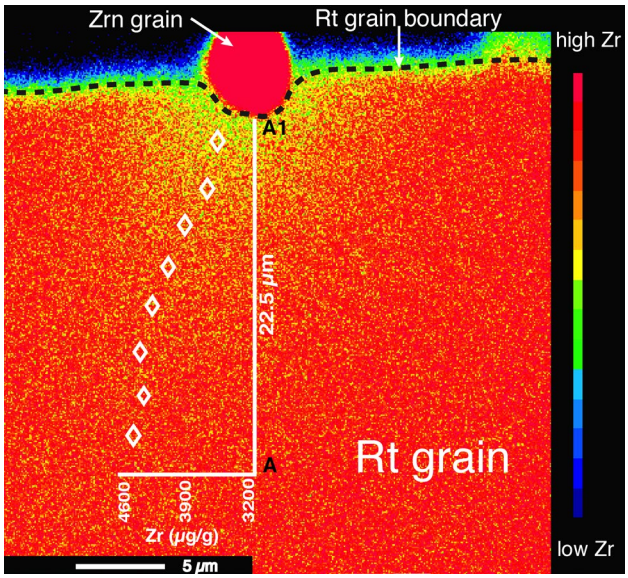

Fig. 9 X-ray intensity map of Zr for rutile grain gRt5 from sample VA10_8a showing the systematic, orbital decrease of Zr in rutile towards grain boundary with adjacent Zrn (*red*). *Colour code* indicates relative Zr concentration from high (*red*) to low (*blue*). A 22.5 µm quantitative EMP concentration profile, carried out over the same area (from A to A1), shows a systematic decrease of Zr from ~4500 to 3600 µg/g. The *dashed line* marks the rutile grain edge

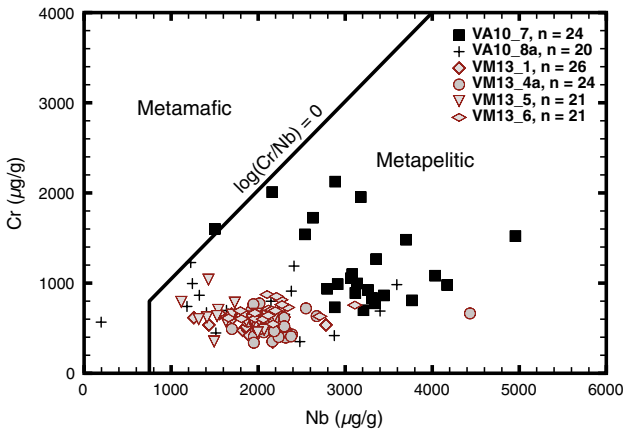

Fig. 10 Nb versus Cr plot to discriminate between metamafic and metapelitic source rock of rutile. Shown are the arithmetic mean values of ~450 individual spot measurements on 136 rutile grains. Discrimination line of the two fields is based on Meinhold (2010)

lower Zr contents and thus lower Zr-in-rutile temperatures of 941–1065 °C.

Trace elements concentration profiles

A total of 18 profiles across 10 different rutile grains from 4 different samples were measured from rutile cores towards rutile grain boundaries with and without adjacent zircons along the grain edges. No systematic variations for Nb, Cr, Al and V were detected for any of the profiles, independently of whether or not the profile was set towards adjacent zircon (Fig. 8b*). In addition, regardless of the main neighbouring phases, Nb, Cr, Al and V concentrations are always homogeneous along the profiles. The Fe concentration in rutile increases towards the rutile grain edges with neighbouring Fe-bearing phases, which is most likely an analytical artefact due to secondary X-ray fluorescence effects.

Rutile grains with adjacent zircons show always a systematic Zr decrease towards the rutile–zircon interface (Fig. 8, Supplementary Fig. S2). These Zr profiles are always smoothly curved and never stepped (Fig. 8, Supp. Fig. S2). Concentration profiles within the same grains but towards rutile grain boundaries without adjacent zircon always display constant Zr (Fig. 8, Supp. Fig. S2). For example, a 30-µm-long concentration profile (VM13_4a_Rt24_Prf1, Supp. Fig. S2) displays a decrease of Zr in the outermost 20–30 µm of the grain towards the rutile–zircon interface from 1200 to 600 µg/g. Spot measurements within the core of this ~150 µm grain yielded Zr concentrations of 1600 µg/g. A second 30-µm-long profile (VM13_4a_Rt24_Prf2) within the same grain, but towards a rutile grain edge devoid of zircon, displays constant Zr concentrations of ~1500 µg/g Zr. Another Zr profile (VM13_6_Rt11_Prf1) is recorded in rutile grain Rt11 from sample VM13_6 (Fig. 8). The Zr concentration decreases from ~1000 to 500 µg/g over a 30-µm-long profile towards the rutile grain edge with adjacent zircon, whereas a second profile (VM13_6_Rt11_Prf2) within the same grain towards the zircon-free grain boundary displays constant Zr concentration of ~900 µg/g (Fig. 8). The systematic decrease of the Zr concentration in rutile towards adjacent zircon is also documented in three more Zr profiles (Supp. Fig. S2) and in a 30 × 30 µm Zr X-ray intensity map, where a Zr depletion halo is visible (Fig. 9). The true decrease of Zr towards adjacent zircon might be slightly stronger as is reflected in the EMP profiles, because of possible X-ray fluorescence effects impacting up on the analyses.

Discussion

Nb, Cr systematics

Some studies report that Nb and Cr contents of rutile can be used to discriminate between rutile growth in a pelitic or in a mafic environment during metamorphism (e.g. Meinhold et al. 2008; Meinhold 2010; Triebold et al. 2007; Zack et al. 2004b), whereas other studies query this potential (e.g. Kooijman et al. 2012; Meyer et al. 2011). The rutile grains investigated in this study display Nb and

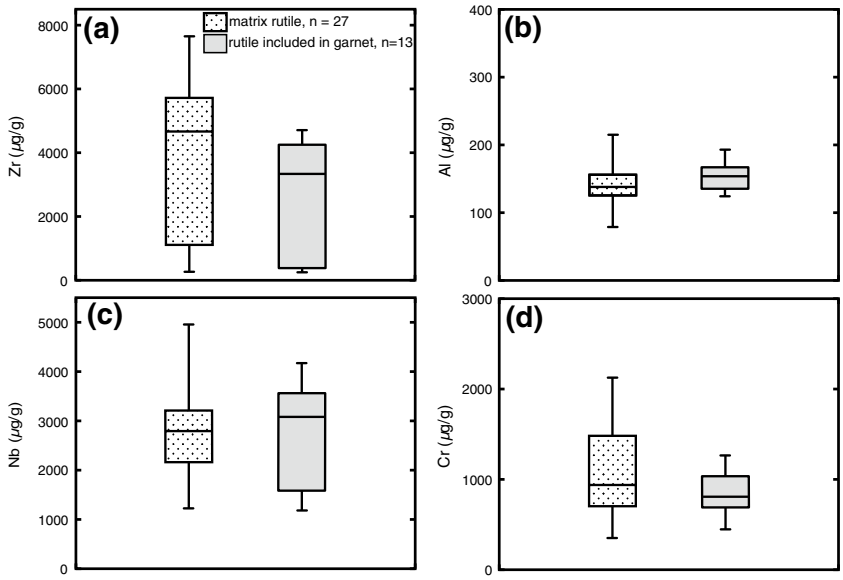

Fig. 11 *Box* and *whisker plots* showing **a** Fe, **b** Nb, **c** Cr and **d** Al contents in matrix rutile compared with concentrations of rutile inclusions within garnet. The *boxes* represent the first to third quartile of data; whiskers represent minimum and maximum values. The *bars* inside the boxes represent the median

Cr concentrations from 200 to 5000 and 340 to 2100 µg/g, respectively (Fig. 6). Neither Cr nor Nb contents correlate systematically with Zr (Fig. 6). The samples from the Val Sesia (VA10) show a larger spread in both, Nb and Cr contents compared to the samples from the Val Mastallone (VM13). When the data are plotted in the Nb–Cr source rock discrimination diagram, all but two rutile grains (98.6 %) plot in the field for metapelites, despite the large variability in Nb and Cr concentrations (Fig. 10). Two studies presented Nb versus Cr data for UHT rutile from Archean rocks, and both pointed out the ambiguity of their results that are not in agreement with the potential of Nb versus Cr source rock discrimination (Meyer et al. 2011; Kooijman et al. 2012). The contrasting results can be interpreted in various ways. Either Nb–Cr source rock discrimination does not generally apply, though it is not clear yet which parameters control whether or not Nb–Cr ratios refer to the source rock; or the Nb–Cr source rock discrimination generally applies but complex metamorphic histories alter the pristine signature as the samples of the two studies showing contrasting results (Meyer et al. 2011; Kooijman et al. 2012) derive from ancient UHT domains and both areas display very heterogeneous geological settings and have undergone complex metamorphic evolution histories. The geological setting and metamorphic history of the rocks from the Ivrea Zone have been studied in detail by numerous authors (e.g. Zingg 1980; Sinigoi et al. 1991; Schnetger 1994; Barboza and Bergantz 2000; Quick et al. 2003) and are now very well understood. Since the investigated rutile crystals clearly grew in metapelitic rocks, the data presented in this study support the potential of source rock discrimination by Nb–Cr content of rutile.

Shielding effect of garnet on the trace element budget of rutile?

Zack et al. (2004a) reported that rutile grains included in garnet commonly preserve the highest Zr content. They argued that rutile inclusions in garnet can be shielded from the rock matrix and protected against diffusive re-equilibration of Zr during cooling. They further concluded that Zr content of rutile inclusions in garnet systematically differs from Zr content of rutile grains in the rocks matrix. In the present study, rutile does not show any systematic correlation between Zr concentrations and textural setting. The Zr concentrations spread over several thousand µg/g for both matrix rutile and rutile included in garnet, with the highest Zr concentrations found in matrix rutile (Fig. 11a). These findings agree with the results of Ewing et al. (2013), who found that Zr-in-rutile temperatures from included rutile are lower than those estimated from rutile grains entrapped or entirely surrounded by e.g. feldspar or quartz. Indeed, the ability of garnet to preserve inclusions from reaction with other minerals is well known from e.g. monazite (Montel et al. 1996; Terry et al. 2000). However, rutile and garnet grow predominantly during prograde metamorphism by biotite breakdown reactions. Consequently, garnet overgrows rutile during prograde metamorphism below peak temperature and not during cooling. If the garnet container prevents Zr re-equilibration in rutile during cooling, it would also prevent early entrapped rutile crystals from equilibrating their Zr content at peak metamorphic conditions. Consequently, rutile inclusions yield Zr contents that correspond to the temperature conditions at the time of their entrapment. The rutile inclusions in garnet from the Ivrea Zone show no systematic high or low Zr

concentration, which suggests continuous rutile and garnet growth during prograde metamorphism. Interestingly, some rutile inclusions in garnet reveal zircon exsolution needles indicating intragranular re-distribution of Zr during cooling. As formation of zircon exsolution from rutile most likely requires the addition of SiO_2 from outside the rutile grain, the garnet container either does not totally shield the rutile from the rock matrix, or the garnet itself provides the Si for zircon formation.

Other trace elements in rutile inclusions in garnet, like Al and Nb, which could give further evidence for shielding effects, show no systematic variations (Fig. 11b, c). Only the Cr content of matrix rutile displays a slightly larger scatter to higher values compared with the Cr content of rutile that occurs as inclusions (Fig. 11d).

Zr systematics in UHT rutile

Diffusion of Zr in Type-III rutile

Many rutile grains that are associated with granular zircon (*Type-III rutile*) record low to medium Zr content compared to the maximum Zr concentration preserved in homogeneous crystals (*Type-I rutile*) from the same samples. Zr concentration in these partly rimmed crystals decreases systematically towards adjacent zircon grains (Figs. 8, 9, Supp. Fig S2). The onset of the decrease occurs steadily at 20–30 μm from the edge of the rutile, regardless of the grain size or the maximum Zr content in the grain centre. Except for the outermost 30 μm, Zr profiles are generally homogeneous across the whole grain. Similar zircon–rutile textures were observed and explained with dissolution–reprecipitation processes affecting these crystals and resetting their Zr-in-rutile temperatures (Ewing et al. 2013). According to this view, recrystallization of rutile at lower temperatures let rutile incorporate less Zr than released during dissolution, resulting in a decrease of Zr towards the rim of the rutile grain, with the released Zr then providing the chemical conditions for zircon crystallization along the rutile rim. This interpretation explains some aspects of the ambiguous Zr profiles and zircon crystals adjacent to rutile, yet some observations need further explanation. Recrystallization of whole up to mm-sized rutile grains at dry HT conditions is unlikely since it could not proceed without dissolution and reprecipitation. The large spread of temperatures recorded in single rock samples is difficult to explain in a model suggesting complete recrystallization of rutile as the temperature spread implies that only some grains would have recrystallized during cooling, whereas others did not and different grains in the same sample recrystallized during different temperature intervals of the retrograde path. If recrystallization would have occurred, one could expect smaller rutile grains to have been more susceptible to complete dissolution and reprecipitation. However, the analysed samples show no correlation between Zr-in-rutile temperature and grain size. During such a process, there is the chance for partial recrystallization of rutile grains. However, neither backscattered electron (BSE) nor secondary electron (SE) imaging reveal textural evidence for partial recrystallization of rutile rims like characteristic former reaction fronts or other heterogeneities. In addition, the trace element distributions in different rutile grains do not reveal any discontinuities, as would be expected across a dissolution–precipitation front. The chemical homogeneity in all trace elements but Zr, the decoupling of Zr-in-rutile temperature and rutile grain size, and the probably dry conditions recorded by the mineral assemblage in the rocks suggests that a recrystallization model—with partial dissolution and reprecipitation of the rutile—is not adequate to explain the modification of primary Zr signatures in Type-III rutile and the decrease of Zr towards rutile–zircon interfaces. An alternative explanation is that tiny parts of rutile rims dissolved without subsequent recrystallization and initiated zircon nucleation along rutile rims during cooling. Rough mass balance calculations show that this process could contribute to crystallization of first zircon nuclei but could not solely explain μm-wide zircon rims. The amount of Zr needed for crystallization of zircon rims would require dissolution of rutile corresponding to 50–120 times the volume of zircon crystallized (calculated for initial Zr concentrations in rutile with 10,000 and 1000 μg/g, respectively). However, the crystallization of first zircon nuclei will enhance Zr diffusion towards the rutile rim. The newly formed zircon provides a sink for Zr and allows equilibration between Zr in rutile and zircon in the presence of quartz during cooling as the Zr does not have to be transported through the rock matrix. Diffusion of Zr in rutile is fast (Sasaki et al. 1985; Cherniak et al. 2007) and thus the primary and prograde zoning of Zr in rutile grown during prograde metamorphism equilibrates, resulting in the flat Zr profiles across rutile with the minor loss of Zr by diffusive along the rim. The two studies that have experimentally investigated Zr diffusion in rutile differ significantly in their results; yet, both suggest quite fast diffusivity for Zr in rutile. Sasaki et al. (1985) determined diffusion constants as a function of oxygen partial pressure (fO_2), crystallographic direction and temperature. Calculating logD for their data at 1100 °C, diffusion of Zr perpendicular to the c-axis is with $\log D = -17.01$ m^2/s slightly faster than diffusion parallel to the c-axis with $\log D = -17.71$ m^2/s. More recently, Cherniak et al. (2007) investigated diffusion of Zr under anhydrous conditions in both natural and synthetic rutile at different fO_2. According to their data, the diffusion coefficient logD for Zr diffusion parallel to the c-axis at $T = 1100$ °C is $\log D = -20.48$ m^2/s, and thus about three orders of magnitude smaller than the diffusion

coefficient calculated from the data of Sasaki et al. (1985). The common preservation of high Zr contents in HT rutile is better explained by slower Zr diffusion, whereas the absence of Zr growth zoning rather indicates fast Zr diffusion. Both experimentally determined diffusivities are too high to account for the limited retrograde Zr diffusion along the outermost rim of the UHT rutiles and are theoretically also too high to support the capability of rutile to preserve UHT Zr signatures—unless unrealistically fast cooling rates are assumed (e.g. Zack et al. 2004a; Watson et al. 2006; Tomkins et al. 2007; Luvizotto and Zack 2009; Kooijman et al. 2012, Ewing et al. 2013). Sasaki et al. (1985) described a strong influence of fO_2 on Zr diffusion depending on temperature and crystallographic direction, which implies that possible variations in fO_2 during metamorphism of the investigated terranes need to be considered as well. As a consequence, care should be taken to compare samples from different HT and UHT terranes in order to evaluate and quantify Zr diffusion in rutile.

Considering only thermodynamics and assuming equilibrium among rutile + zircon + quartz at any given moment, all rutile grains that equilibrated their Zr contents during prograde or peak metamorphic conditions would adjust their Zr concentrations during cooling. However, rutile retains high concentrations of Zr providing evidence that high temperatures were attained at some point during the thermal evolution of the host rock (e.g. Luvizotto and Zack 2009; Jiao et al. 2011; Meyer et al. 2011; Kooijman et al. 2012; Ewing et al. 2013; Korhonen et al. 2014; Smye and Stockli 2014). This feature suggests that kinetics play an important role. Instead of the intragranular transport of Zr in rutile restricting equilibration, it might be the limited mobility of ZrO_2 or SiO_2 in the rock matrix (an intergranular problem) that governs the equilibration between the phases. Taylor-Jones and Powell (2015) proposed a theoretical approach of Si diffusion in rutile and its possible influence on the preservation of Zr in rutile acknowledging that SiO_2 is known to be one of the least mobile species (Béjina and Jaoul 1997). Diffusion constants for Si in rutile, which are required to calculate Si closure temperatures, have not been experimentally determined yet. However, Taylor-Jones and Powell (2015)computed closure temperatures for Si in rutile using theoretical values for E_A and D_0 which they inferred from a compensation trend for Si diffusion in silicates presented by Brady and Cherniak (2010). Even though the approach is somewhat speculative, it is useful to discuss a probable influence of Si diffusion in rutile on the behaviour of Zr in rutile. For any given grain size and cooling rate, Si closure temperatures might be several 100 °C higher than the closure temperatures for Zr in rutile. If so, the interaction between rutile (or the Zr in rutile) and other phases stops once the temperature has decreased below Si closure—which will always be far above Zr closure temperature. From that moment on, the thermodynamic basis of the Zr-in-rutile thermometer, which is the equilibrium rutile + zircon + quartz, is not any longer valid, allowing rutile to retain high Zr concentrations. Combined with the relatively fast diffusivity of Zr in rutile, this helps to understand the nearly homogeneous Zr profiles in single grains. However, the presence of zircon exsolutions in some rutile grains while totally absent in other grains remains unclear when focusing only on Si closure in rutile.

Baddeleyite exsolution from Type-II rutile with subsequent zircon formation

The oriented zircon needles found in some ultra-high temperature (UHT) rutiles are collectively interpreted as zircon exsolutions from the rutile host (e.g. Zack et al. 2004a; Watson et al. 2006; Kooijman et al. 2012). Spatial and textural relationships between rutile and Zr-bearing exsolutions indeed indicate that zircon needles source the Zr from their rutile host. Some repeated features observed for all the zircon needles analysed in this study seem to be specific and characteristic for their formation processes: (1) all rutile crystals that contain zircon exsolution needles (Type-II) have low Zr concentrations of 200–500 µg/g between exsolved zircon, corresponding to Zr-in-rutile temperatures of 630–700 °C. (2) Zr concentrations of the rutile matrix in between zircon needles are always homogeneous on a µm scale and do not change towards zircon (Fig. 7). (3) Zircon exsolution needles do not vary significantly in size—neither in length nor in width—within single and between different rutile grains. (4) Zircon exsolution needles mostly show shape-preferred orientations (SPO) in different directions controlled by their rutile host crystal with a prominent orientation being Zrn[001]//Rt {110}. (5) Zircon exsolution needles commonly show crystallographic preferred orientations (CPO) (unpublished data, this study). Therefore, it can be ruled out that zircon needles in rutile are inclusions that grew before their host grains and were entrapped during rutile growth.

Of all investigated rutile crystals containing exsolutions, one grain was found to contain lamellae-like baddeleyite (ZrO_2) instead of zircon (Fig. 2f), indicating that zircon exsolutions in rutile do not form by direct exsolution of $ZrSiO_4$ but through the intermediate step of expulsion of ZrO_2. For zircon formation, the exsolved ZrO_2 subsequently reacts with SiO_2 to form zircon according to the reaction:

$$ZrO_{2(\text{exsolved baddeleyite})} + SiO_2 = ZrSiO_{4(\text{zircon exsolution needle})}$$

Yet, the source of Si required for the reaction and the temperature of this reaction need to be established. The Zr-in-rutile temperatures of 630–700 °C recorded in the matrix of all rutile grains with zircon exsolution needles imply that

equilibration of Zr in rutile and formation of zircon exsolution needles proceeded until temperatures down to 630 °C were attained.

If the closure temperature for Si diffusion in rutile is high and well above the Zr closure (Taylor-Jones and Powell 2015), the zircon-forming reaction should be restricted to very high temperatures, especially if the Si originates from outside the rutile grain. However, as long as no experimental data on Si diffusion in rutile are available, this issue remains speculative. Microprobe measurements have failed to detect systematic differences in the Si concentrations of rutile matrix with or without zircon exsolution needles. This suggests that the formation of zircon from baddeleyite required Si to come from outside the rutile grains. The nearby presence of quartz is, however, apparently not the main prerequisite for SiO_2 availability, since the only rutile grain that preserved baddeleyite occurs as inclusion within quartz. Due to the general low mobility of SiO_2, it is likely the absence or presence of a fluid to transport the Si. Undamaged quartz crystals hardly allow fluids to pass through their structure, which led to the preservation of metastable baddeleyite exsolutions within the rutile crystal included in quartz. The intra-grain mobility of Si in rutile, which is needed to form zircon from baddeleyite, is facilitated by structural defects that result from the exsolution of baddeleyite. Nanoscale dislocations and misfits between baddeleyite exsolutions and host grains are generally known to be the result of exsolution processes, and they will provide excellent pathways for Si transport. It is thus the ZrO_2 exsolution process itself, which enforces the later fluid-supported in-diffusion of Si into rutile. Future TEM studies are needed to detect former fluid pathways to test this hypothesis further.

Reconstructing peak T by mathematical and analytical reintegration of zircon exsolutions

Since zircon needles in rutile are the product of exsolution of ZrO_2, its reintegration yields the Zr concentration of the rutile host grains prior to the exsolution. We selected the rutile crystals that provided the most regular and homogeneously distributed zircon needles for mathematical and analytical reintegration (e.g. Fig. 3b, c). Although this approach is based on the two-dimensional distribution of zircon needles using BSE and SE images, the regular distribution of zircon needles observed in rutiles grains cut in various crystallographic orientations suggests that zircon exsolution needles are homogeneously distributed within the whole rutile grains (Fig. 3).

The mathematical reintegration of zircon needles reveals initial Zr concentrations of ~1.2–2 wt%, equivalent to Zr-in-rutile temperatures of 1085–1194 °C (Table 1). These temperatures are extremely high compared to other UHT-areas and are higher than previously reported Zr-in-rutile temperatures from the same area that were determined by LA-ICP-MS analyses (Ewing et al. 2013). Due to the exponential increase of Zr incorporation in rutile with increasing temperature, the estimated volume of exsolved zircon is the major factor controlling the mathematically integrated temperatures. This volume could be overestimated due to e.g. brightness effects in the BSE images, or if zircon exsolutions contain unrecognized sub-micron-sized minor oxide phases. Electron backscatter diffraction studies (unpublished data), EDX mapping and comprehensive Raman analyses on the investigated samples reveal that zircon exsolutions typically range in thickness from 300 to 700 nm and never reveal other minor phases associated with them.

The analytical reintegration of zircon exsolution needles by 60 µm defocused beam microprobe analyses results in systematically lower Zr-in-rutile temperatures of 940–1060 °C (Fig. 12). The results of these analyses are, however, biased towards lower temperatures by numerous effects. Rutile and zircon differ in their chemistry, crystal structure and density. Both phases have different absorption coefficients resulting in different characteristic X-ray efficiencies. Possible fluorescence effects due to zircon in rutile and the difference of the incident angle of the electrons at the centre and at the periphery of the spot bias the analyses. Summing up these effects, the analytically integrated Zr concentration will be underestimated resulting in systematically low Zr-in-rutile temperatures. It is unfortunately not possible to quantify the underestimation of Zr-in-rutile temperatures by analytical reintegration. The temperatures of 940–1060 °C are therefore treated as absolute minimum temperatures for peak metamorphic conditions, indicating that the true peak temperatures must be higher.

Although uncertainties in the estimated volume of zircon exsolution are expected and inevitable, the mathematically calculated temperatures of 1085–1194 °C are nevertheless in good agreement with the thermal history of the selected samples and likely reflect the best estimates of the peak metamorphic conditions. The studied samples were collected in centimetre to decimetre thick metapelitic bands (paragneiss septae) from the Kinzigite Formation that underwent regional granulite facies metamorphism already before being subsequently affected by the contact metamorphic overprint during the emplacement of the Mafic Complex. During this major magmato-thermal event, the paragneiss septae were intruded and surrounded by basaltic magma for which a temperature of 1200–1250 °C is a realistic estimate. Parts of the dry and restitic metapelites were completely immersed in the basaltic magma and thus could have reached the basalt melt temperature. As the reintegrated Zr-in-rutile temperatures never exceed temperatures of 1200 °C, and taking into account the thermal history of

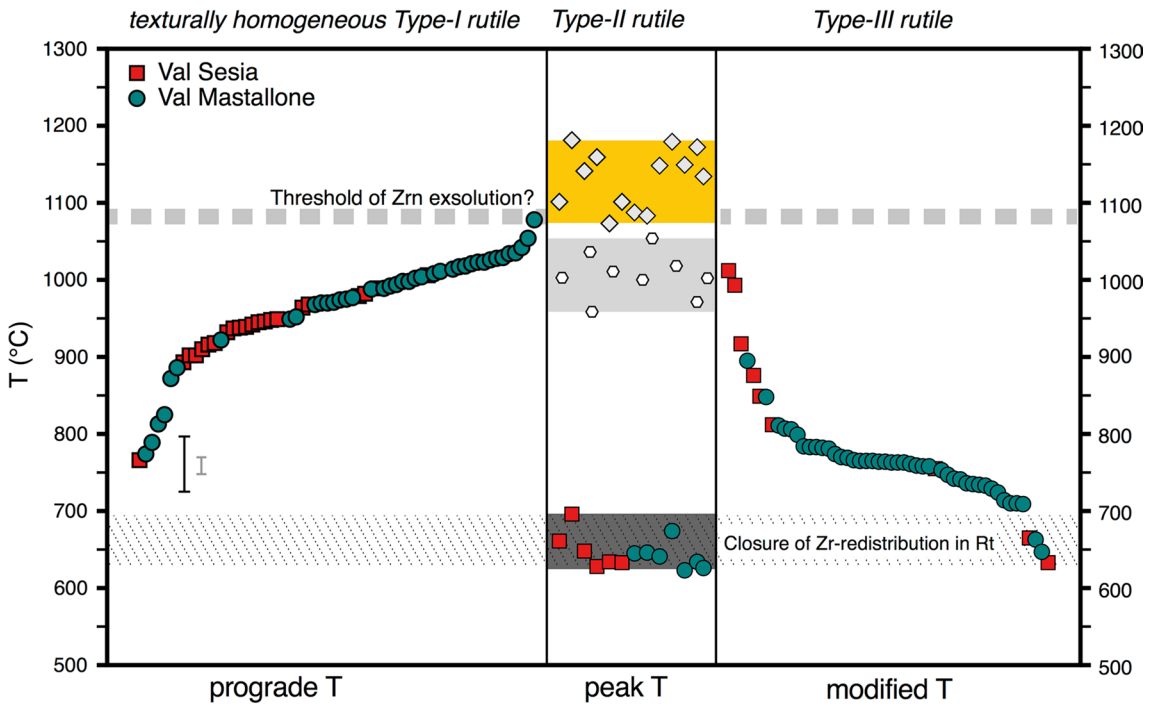

Fig. 12 Zr-in-rutile temperatures separated in three different groups based on textural distinct types of crystals and sorted by temperature. *Teal circles* and *red squares* indicate Zr-in-rutile temperatures of Val Mastallone and Val Sesia rutile, respectively. Hexagons (*grey band*) indicate analytically reintegrated and diamonds (*yellow band*) indicate mathematically reintegrated Zr-in-rutile temperatures. The Zr threshold of Zrn exsolution and the low T band of Zr closure in Rt are marked as *grey dashed line* and dotted area, respectively. The *x*-axis indicates the proposed link between Zr-in-rutile temperatures and relative timing of the metamorphic evolution, with prograde-, peak- and retrograde metamorphism. For the sake of clarity, *error bars* are not shown for individual samples. The *grey* and *black error bars* represent the error on Zr-in-rutile temperatures at 750 °C considering analytical uncertainties only (*grey*) and total error (*black*), respectively

the collected samples, the temperatures of 1085–1194 °C are geologically realistic. Consequently, these temperatures are interpreted as the peak metamorphic temperatures for the lower parts of the Kinzigite Formation of the Ivrea Zone that were stepwise immersed in the basaltic magma of the Mafic Complex (Table 1; Fig. 12). They reflect the unique geological settings and metamorphic conditions of the lowest continental crustal section of the Ivrea Zone.

The reintegration not only recovers the peak temperatures of the investigated samples but also reveals that exsolution in the investigated samples most probably only occurred when initial Zr concentrations exceeded ~1.1 wt% (~1085 °C), while no exsolution-free rutile grain recording Zr concentrations higher than 1.0 wt% (~1050 °C) was found. This suggests a threshold of 1.1 wt% above which rutile could not retain its Zr and started to exsolve baddeleyite during cooling. As only rutile grains showing absolutely regular and homogeneously distributed exsolution, needles were used for reintegration, it should be noted that the reintegration for other rutile crystals could result in lower initial Zr contents, which would lower the threshold of 1.1 wt% Zr or even make it invalid. Beside the initial Zr content, additional aspects might control the onset of exsolution or prevent it e.g. the post-peak metamorphic evolution—particularly the cooling rates of samples, microstructural defects, the presence of a (hydrous) fluid during cooling or the presence of water in nominally anhydrous minerals. Degeling (2002) presented integrated Zr-in-rutile temperatures for rutile samples from the Napier Complex containing zircon exsolutions, some of which are significantly lower than temperatures obtained from homogeneous grains from the same samples. Since the mechanisms and necessary conditions for the onset of exsolution during cooling from high temperature are not known, the threshold for zircon exsolution suggested here may not necessarily apply to samples from other high-grade terranes.

Prograde and retrograde temperature evolution recorded by Zr in rutile

In the frequency histograms (Fig. 5a–g), all analysed rutile grains were plotted, regardless of whether the rutile was homogeneous (Type-I), contained zircon needles (Type-II) or contained or was rimmed by granular zircon (Type-III). Additionally, no integrated temperatures are considered in the histograms. Hence, these temperatures reflect a combination of (prograde) equilibration temperatures and more or less reset temperatures, and therefore, these temperatures

can only be interpreted in a petrogenetic context. Since rutile grains that are partially rimmed by zircon never provide fully equilibrated Zr-in-rutile temperatures (as shown by the Zr diffusion profiles), the temperatures obtained from the cores of such grains cannot easily be linked to a specific stage of the metamorphic history of the rock. The Zr-in-rutile temperatures from the core regions of such grains (Type-III) range from 650 to 950 °C (Fig. 12). In contrast to homogeneous (Type-I) rutile grains, these grains are in direct contact with zircon (along the rims), which provided a sink for Zr and enabled diffusional loss of Zr during cooling. The texturally homogeneous Type-I rutile grains, which are free of both zircon exsolution and zircon at the rim, show no textural or chemical evidence that support re-equilibration of Zr. Additionally, these grains show homogeneously distributed Zr, Nb, Cr, Al and Fe and reveal no growth zoning or diffusive loss of Zr in EMP concentration profiles. Thus, the different temperatures recorded by different homogeneous Type-I rutile grains from the same sample correspond to the thermal condition during their growth and the different temperatures then preserve evidence for different rutile producing reactions during the prograde path. Since there is no correlation between trace element content (Nb, Cr. Fe, Al, Fig. 6) and Zr-in-rutile temperatures, it is likely that the rutile grains all formed as a result of biotite breakdown during the prograde path, but different sub-parageneses in the same sample reacted to form rutile at different temperatures.

Nearly all of these homogeneous grains record distinct high temperatures of 900–1000 °C in samples from the Val Sesia and 950–1050 °C in samples from Val Mastallone, with only five grains recording temperatures significantly lower than 900 °C (760–840 °C) (Fig. 12). Rutile grains with equilibration Zr temperatures below 1050 °C retained their Zr, stayed homogeneous and thus record their growth temperatures during the prograde path. Figure 5h shows a temperature histogram of all analysed samples, including the reintegrated peak temperatures and the pooled results based on rutile texture.

Conclusions

The comprehensive set of metamorphic rutile crystals in metapelites from the lowermost part of the Ivrea Zone reveals the behaviour of the Zr-in-Rt thermometer during the prograde and retrograde path that reached UHT conditions and is suitable to evaluate its robustness during prograde and retrograde metamorphism. A key observation is that rutile grains with the same P–T history show quite diverse textures and a wide range in Zr concentrations that translate into a wide range in apparent formation or equilibration temperatures. Experimental studies show that diffusion of Zr is quite fast, and equilibration after UHT metamorphism is to be expected. This is consistent with the general observation that prograde growth zonation in rutile grains cannot be observed. However, this equilibration affects only the intragranular distribution of Zr in single rutile grains. Limited transport of Zr between minerals and very slow Si diffusion within rutile generally prevent Zr re-equilibration with other minerals during cooling. The differences in textural relations between rutile grains and adjacent or included zircon in UHT samples indicate variable processes of Zr redistribution in rutile following peak metamorphic conditions. The different bulk Zr concentrations of individual rutile grains in the same sample are evidence for the lack of Zr exchange with the surrounding rock matrix during the metamorphic evolution, an observation that contrasts with the behaviour of the U–Pb system in rutile. The different Zr contents imply that rutile grains in these layered pelitic gneisses grew in an environment where not enough Zr was available during mineral reaction, or at different intervals during the prograde metamorphism, and thus rutile kept the information on the time integrated temperature interval of its growth. Rutile grains with extensive exsolution (Type-II) of zircon or rare baddeleyite record the highest temperatures if the exsolved zircon is re-integrated. These zircon needles formed when baddeleyite exsolved from rutile during cooling and subsequently reacted with SiO_2—probably derived from outside the rutile grains. The exsolution proceeded down to temperatures of 630–700 °C, which corresponds to the closure temperatures for intracrystalline Zr redistribution in rutile. The reintegration of zircon exsolution needles results in temperatures of up to 1190 °C which is similar to the melt temperature of the surrounding gabbro and reflects the peak metamorphic temperature in the septae of the Mafic Complex in the Ivrea Zone. The preservation of such high temperatures by Zr-in-rutile thermometry makes this solution thermometer indeed a powerful geothermometer to recover peak conditions during UHT metamorphism if post-metamorphic-peak modifications such as exsolution of zircon or baddeleyite and minor granular exsolution along the grain boundaries are taken into account. The preservation of these various temperature information in grains with extensive exsolution of zircon implies that the texturally homogeneous Type-I rutile grains with relatively low Zr contents do not indicate retrograde modification of Zr but record prograde rutile growth from temperatures of 750–1080 °C. Thus, the different Zr concentrations in rutile crystals from the same sample provide a record of prograde metamorphic reactions and the distinct equilibration textures developed in individual grains are an effect of retrograde adjustment.

Acknowledgments We gratefully thank T. Zack for providing a piece of rutile standard R10b. T. Pettke is thanked for the help with La-ICP-MS analysis. E. Axelsson is acknowledged for helpful discussion. Furthermore, we thank T. Zack, E. B. Watson and an anonymous reviewer for their helpful comments, which improved the quality of the manuscript, and J. Hoefs for the editorial handling.

References

Armstrong JT (1995) CITZAF: a package of correction programs for the quantitative electron microbeam X-ray analysis of thick polished materials, thin films, and particles. Microbeam Anal 4:177–200

Barboza SA, Bergantz GW (2000) Metamorphism and anatexis in the mafic complex contact aureole, Ivrea zone, northern Italy. J Petrol 41:1307–1327

Barboza SA, Bergantz GW, Brown M (1999) Regional granulite facies metamorphism in the Ivrea zone: is the Mafic Complex the smoking gun or a red herring? Geology 27:447–450

Béjina F, Jaoul O (1997) Silicon diffusion in silicate minerals. Earth Planet Sci Lett 153(3–4):229–238

Bohlen SR, Liotta JJ (1986) A barometer for garnet amphibolites and garnet granulites. J Petrol 27:1025–1034

Bohlen SR, Wall VJ, Boettcher AL (1983) Experimental investigations and geological applications of equilibria in the system $FeO–TiO_2–Al_2O_3–SiO_2–H_2O$. Am Mineral 68:1049–1058

Brady JB, Cherniak DJ (2010) Diffusion in minerals: an overview of published experimental diffusion data. In: Zhang Y, Cherniak DJ (eds) Reviews in mineralogy and geochemistry, vol 72., Diffusion in minerals and meltsMineralogical Society of America and Geochemical Society, Chantilly, pp 899–920

Cherniak DJ, Manchester J, Watson EB (2007) Zr and Hf diffusion in rutile. Earth Planet Sci Lett 261(1–2):267–279

Degeling H (2002) Zircon equilibria in metamorphic rocks. Unpublished Ph.D. thesis, ANU

Ewing TA, Rubatto D, Hermann J (2013) The robustness of the Zr-in-rutile and Ti-in-zircon thermometers during high-temperature metamorphism (Ivrea–Verbano Zone, northern Italy). Contrib Mineral Petrol 165:757–779

Ferry JM, Watson EB (2007) New thermodynamic models and revised calibrations for the Ti-in-zircon and Zr-in-rutile thermometers. Contrib Mineral Petrol 154(4):429–437

Guillong M, Meier DL, Allan MM, Heinrich CA, Yardley BWD (2008) SILLS: a MATLAB-based program for the reduction of laser ablation ICP-MS data of homogeneous materials and inclusions. Mineral Assoc Canada Short Course 40:328–333

Harley SL (1989) The origin of granulites: a metamorphic perspective. Geol Mag 126:215–247

Harley SL, Motoyoshi Y (2000) Al zoning in orthopyroxene in a sapphirine quartzite: evidence for >1120 °C UHT metamorphism in the Napier Complex, Antarctica, and implications for the entropy of sapphirine. Contrib Mineral Petrol 138:293–307

Henk A, Franz L, Teufel S, Oncken O (1997) Magmatic underplating, extension, and crustal reequilibration: insights from a cross-section through the Ivrea Zone and Strona–Ceneri Zone, Northern Italy. J Geol 105(3):367–377

Jiao S, Guo J, Mao Q, Zhao R (2011) Application of Zr-in-rutile thermometry: a case study from ultrahigh-temperature granulites of the Khondalite belt, North China Craton. Contrib Mineral Petrol 162(2):379–393

Jochum KP et al (2011) Determination of reference values for NIST SRM 610–617 glasses following ISO guidelines. Geostand Geoanal Res 35(4):397–429

Kooijman E, Smit MA, Mezger K, Berndt J (2012) Trace element systematics in granulite facies rutile: implications for Zr geothermometry and provenance studies. J Metamorph Geol 30:397–412

Korhonen FJ, Clark C, Brown M, Taylor RJM (2014) Taking the temperature of Earth's hottest crust. Earth Planet Sci Lett 408:341–354

Luvizotto GL, Zack T (2009) Nb and Zr behavior in rutile during high-grade metamorphism and retrogression: an example from the Ivrea–Verbano Zone. Chem Geol 261:303–317

Luvizotto GL, Zack T, Meyer HP, Ludwig T, Triebold S, Kronz A, Münker C, Stockli DF, Prowatke S, Klemme S, Jacob DE, von Eynatten H (2009) Rutile crystals as potential trace element and isotope mineral standards for microanalysis. Chem Geol 261:346–369

Meinhold G (2010) Rutile and its applications in earth sciences. Earth Sci R 102:1–28

Meinhold G, Anders B, Kostopoulos D, Reischmann T (2008) Rutile chemistry and thermometry as provenance indicator: an example from Chios Island, Greece. Sediment Geol 203:98–111

Meyer M, John T, Brandt S, Klemd R (2011) Trace element composition of rutile and the application of Zr-in-rutile thermometry to UHT metamorphism (Epupa Complex, NW Namibia). Lithos 126(3–4):388–401

Montel J-M, Foret S, Veschambre M, Nicollet C, Provost A (1996) Electron microprobe dating of monazite. Chem Geol 131:37–53

Peressini G, Quick JE, Sinigoi S, Hofmann AW, Fanning M (2007) Duration of a large Mafic intrusion and heat transfer in the lower crust: a SHRIMP U–Pb zircon study in the Ivrea–Verbano Zone (Western Alps, Italy). J Petrol 48:1185–1218

Pettke T, Oberli F, Audetat A, Guillong M, Simon AC, Hanley JJ, Klemm LM (2012) Recent developments in element concentration and isotope ratio analysis of individual fluid inclusions by laser ablation single and multi collector ICP-MS. Ore Geol Rev 44:10–38

Quick JE, Sinigoi S, Mayer A (1995) Emplacement of mantle peridotite in the lower continental crust, Ivrea–Verbano Zone, northwest Italy. Geology 23:739–742

Quick JE, Sinigoi S, Snoke AW, Kalakay TJ, Mayer A, Peressini G (2003) Geologic map of the Southern Ivrea–Verbano Zone, Northwestern Italy. Geologic Investigations Series Map I-2776 and booklet (22 p). US Geological Survey, U.S. Government Printing Office

Redler C, Johnson TE, White RW, Kunz BE (2012) Phase equilibrium constraints on a deep crustal metamorphic field gradient: metapelitic rocks from the Ivrea Zone (NW Italy). J Metamorph Geol 30(3):235–254

Sasaki J, Peterson NL, Hoshino K (1985) Tracer impurity diffusion in single-crystal rutile (TiO2-x). J Phys Chem Solids 46:1267–1283

Schmitt AK, Zack T (2012) High-sensitivity U–Pb rutile dating by secondary ion mass spectronomy (SIMS) with an O2 + primary beam. Chem Geol 332–333:65–73

Schnetger B (1994) Partial melting during the evolution of the amphibolite-facies to granulite-facies gneisses of the Ivrea Zone, northern Italy. Chem Geol 113:71–101

Schuster R, Stüwe K (2008) Permian metamorphic events in the Alps. Geology 36:603–606

Sinigoi S, Antonini P, Demarchi G, Longinell A, Mazzucchelli M, Negrini L, Rivalenti G (1991) Intractions of mantle and crustal magmas in the southern part of the Ivrea Zone (Italy). Contrib Mineral Petrol 108(4):385–395

Sinigoi S, Quick JE, Mayer A, Demarchi G (1995) Density-controlled assimilation of underplated crust, Ivrea–Verbano Zone, Italy. Earth Planet Sci Lett 129:183–191

Sinigoi S, Quick JE, Mayer A, Budahn J (1996) Influence of stretching and density contrasts on the chemical evolution of continental magmas: an example from the Ivrea–Verbano zone. Contrib Mineral Petrol 123:238–250

Smye AJ, Stockli DF (2014) Rutile U–Pb age depth profiling: a continuous record of lithospheric thermal evolution. Earth Planet Sci Lett 408:171–182

Taylor-Jones K, Powell R (2015) Interpreting zirconium-in-rutile thermometric results. J Metamorph Geol 33:115–122

Terry MP, Robinson P, Krogh-Ravna EJ (2000) Kyanite eclogite thermobarometry and evidence for thrusting of UHP over HP metamorphic rocks, Nordoyane, Western Gneiss Region, Norway. Am Mineral 85:1637–1650

Tomkins HS, Powell R, Ellis DJ (2007) The pressure dependence of the zirconium-in-rutile thermometer. J Metamorph Geol 25:703–713

Triebold S, Von Eynatten H, Luvizotto G, Zack T (2007) Deducing source rock lithology from detrital rutile geochemistry: an example from the Erzgebirge, Germany. Chem Geol 244:421–436

Watson EB, Wark DA, Thomas JB (2006) Crystallization thermometers for zircon and rutile. Contrib Mineral Petrol 151:413–433

Zack T, Moraes R, Kronz A (2004a) Temperature dependence of Zr in rutile: empirical calibration of a rutile thermometer. Contrib Mineral Petrol 148:471–488

Zack T, von Eynatten H, Kronz A (2004b) Rutile geochemistry and its potential use in quantitative provenance studies. Sediment Geol 171(1):37–58

Zingg A (1980) Regional Metamorphism in the Ivrea Zone (Southern Alps, N-Italy): field and microscopic investigations. Schweiz Mineral Petrogr Mitt 60:153–179